© 2017. Published by The Company of Biologists Ltd | Development (2017) 144, 151-162 doi:10.1242/dev.141325

RESEARCH ARTICLE

Modulation of apical constriction by Wnt signaling is required for lung epithelial shape transition

Katsumi Fumoto[1], Hisako Takigawa-Imamura[2], Kenta Sumiyama[3], Tomoyuki Kaneiwa[1] and Akira Kikuchi[1,*]

ABSTRACT

In lung development, the apically constricted columnar epithelium forms numerous buds during the pseudoglandular stage. Subsequently, these epithelial cells change shape into the flat or cuboidal pneumocytes that form the air sacs during the canalicular and saccular (canalicular-saccular) stages, yet the impact of cell shape on tissue morphogenesis remains unclear. Here, we show that the expression of Wnt components is decreased in the canalicular-saccular stages, and that genetically constitutive activation of Wnt signaling impairs air sac formation by inducing apical constriction in the epithelium as seen in the pseudoglandular stage. Organ culture models also demonstrate that Wnt signaling induces apical constriction through apical actomyosin cytoskeletal organization. Mathematical modeling reveals that apical constriction induces bud formation and that loss of apical constriction is required for the formation of an air sac-like structure. We identify MAP/microtubule affinity-regulating kinase 1 (Mark1) as a downstream molecule of Wnt signaling and show that it is required for apical cytoskeletal organization and bud formation. These results suggest that Wnt signaling is required for bud formation by inducing apical constriction during the pseudoglandular stage, whereas loss of Wnt signaling is necessary for air sac formation in the canalicular-saccular stages.

KEY WORDS: Epithelium, Wnt, Apical constriction, Mark1, Mouse

INTRODUCTION

The mammalian lung develops through four consecutive stages: the pseudoglandular, canalicular, saccular and alveolar stages (Chao et al., 2015). During the pseudoglandular stage [embryonic day (E) 9.5 to E16.5], lung epithelium shows stereotypical branching morphogenesis and columnar epithelial cells dynamically change their shape when new buds arise (Kadzik et al., 2014; Metzger et al., 2008). During the subsequent canalicular and saccular (canalicular-saccular) stages (from E16.5 to postnatal day 5), air sacs emerge at the distal end surrounded by capillaries, and the lung epithelium differentiates into a mixture of cuboidal type II and flat squamous type I pneumocytes. Signaling pathways for branching morphogenesis have been well established. Fibroblast growth factor 10 (FGF10) is expressed in the distal mesenchyme and induces lung bud formation. Bone morphogenetic protein 4 (BMP4) is induced by FGF10 and locally restricts endodermal outgrowth, thereby inducing lateral outgrowth (Morrisey and Hogan, 2010; Weaver et al., 2000). During the alveolar stage, myofibroblasts stimulated by vascular endothelial growth factor (VEGF) from type I pneumocytes play a crucial role in the formation of the secondary septa (Yang et al., 2016). Thus, although the molecular mechanisms of branching morphogenesis and alveologenesis have been well studied, it is less clear how epithelial cells change their morphology from columnar cells during the pseudoglandular stage to flat and cuboidal cells during the canalicular-saccular stages, and whether their specific cell shapes are required for bud formation in the former stage and air sac formation in the latter stages.

During early lung development, several Wnt ligands are expressed in both epithelial and mesenchymal cells. There are two different pathways induced by Wnt signaling: the β-catenin pathway and the β-catenin-independent pathway. In the former pathway, Wnt signaling induces gene expression through β-catenin stabilization, and in the latter pathway, Wnt signaling regulates cell motility and polarity through cytoskeletal organization (Kikuchi et al., 2011). Wnt2 and Wnt2b are expressed in the lung mesenchyme and play a pivotal role in lung endoderm specification, as their loss results in lung agenesis (Goss et al., 2009). Wnt7b is exclusively expressed in the lung epithelium and is required for vascular system formation by inducing smooth muscle cell proliferation (Cohen et al., 2009; Shu et al., 2002). Wnt2 and Wnt7b are cooperatively required for the mesenchymal β-catenin pathway in cultured cell lines and their simultaneous knockout causes defects in branching morphogenesis and proximal-distal specification (Miller et al., 2012). The β-catenin pathway is consistently activated in the distal endodermal tip and surrounding mesenchyme during the early stage of lung development, as observed in a reporter gene-expressing murine model (Al Alam et al., 2011), and is required for branching morphogenesis (De Langhe et al., 2005; Miller et al., 2012) as well as distal progenitor maintenance (Mucenski et al., 2003). Although these studies reveal the importance of Wnt signaling in lung development, it remains unclear how the β-catenin pathway is involved in epithelial cell morphogenesis during lung development. Here, we investigated the role of Wnt signaling in lung epithelial morphogenesis during the transition from the pseudoglandular to the saccular-canalicular stages.

RESULTS

The apical actomyosin cytoskeleton in the lung epithelium is reorganized during the transition from the pseudoglandular to the canalicular-saccular stages

Apical constriction is involved in bud formation during the pseudoglandular stage in vertebrate lung development (Kadzik et al., 2014; Kim et al., 2013). Contractile activity at the apical cell surface was visualized with phospho-threonine-18 and serine-19 myosin II light chain (ppMLC). Whereas ppMLC was dominantly localized to the apical cell surface and adherens junctions at E14.5 (the pseudoglandular stage), ppMLC was decreased and found

[1]Departments of Molecular Biology and Biochemistry, Graduate School of Medicine, Osaka University, 2-2 Yamadaoka, Suita 565-0871, Japan. [2]Anatomy and Cell Biology, Graduate School of Medical Sciences, Kyushu University, Fukuoka 812-8582, Japan. [3]Laboratory for Mouse Genetic Engineering, RIKEN Quantitative Biology Center, 1-3 Yamadaoka, Suita, Osaka 565-0871, Japan.

*Author for correspondence (akikuchi@molbiobc.med.osaka-u.ac.jp)

A.K., 0000-0003-3378-9522

Received 21 June 2016; Accepted 21 November 2016

Development (2017) 144, 151-162 doi:10.1242/dev.141325

throughout the cytoplasm at E17.5 (the canalicular-saccular stages) (Fig. 1A,B). Concomitantly, F-actin was enriched at the apical surface and adherens junctions at E14.5 but was distributed to the basolateral cortex at E17.5 (Fig. 1A,B). When the location of tension generated by actomyosin contractility was assessed with α18, an antibody that recognizes a form of α-catenin that is conformationally changed by actomyosin-mediated forces (Yonemura et al., 2010), a strong signal was detected locally at adherens junctions but not the lateral membrane at E14.5, indicating that tension is generated around the apical perimeter (Fig. 1C,D). This apically restricted α18 signal was diminished by E17.5 and redistributed to the basolateral cortex (Fig. 1C,D).

To confirm apical cytoskeletal reorganization, an apically localized protein that anchors the actomyosin cytoskeleton to the apical cortex was assessed. In the E14.5 lung, podocalyxin (Podxl), an apically localized transmembrane protein (Bryant et al., 2014), was clearly localized to the apical cortex of columnar-shaped cells in the distal end of the epithelium (Fig. 1E). In the E17.5 lung, podocalyxin localization to the apical cortex in both cuboidal and flat squamous-shaped cells was decreased and detected in the cytoplasm and basolateral cortex (Fig. 1E,H). Additionally, cells positive for podoplanin (Pdpn), a type I pneumocyte marker, or SP-C (Sftpc), a type II pneumocyte marker, lost apical podocalyxin localization, indicating that the apical actin cytoskeleton is globally reorganized during the canalicular-saccular stages (Fig. 1F-H).

Sftpc and *Pdpn* mRNA levels were significantly increased in the distal end of the E18.5 lung compared with that of the E14.5 lung (Fig. S1). At E18.5, among Wnt signaling components, *Wnt7b*, the Wnt receptors *Fz1* (*Fzd1*), *Fz7* (*Fzd7*) and *Fz10* (*Fzd10*), and the β-catenin pathway target genes *Lef1* and *Dkk1* were significantly decreased whereas other signaling molecules, including *Bmp4*, *Fgf9* and *Fgf10*, were not (Fig. S1) (Wang et al., 2005). These findings prompted us to examine the possible involvement of Wnt signaling in the apical cytoskeleton reorganization during lung development.

The β-catenin pathway induces bud formation and is required for apical cytoskeleton organization

To examine whether modulation of the β-catenin pathway is required for apical cytoskeleton reorganization *in vivo*, *Ctnnb1*$^{(Ex3)fl/fl}$ mice, in which exon 3 of the β-catenin gene (*Ctnnb1*) is flanked by loxP sites (Harada et al., 1999) were crossed with *Ctnnb1*$^{(Ex3)fl/fl}$; *Rosa26-Cre/ERT2Tg* [hereafter *Ctnnb1*$^{(Ex3)fl/fl}$*;Cre*] mice. By administering tamoxifen to pregnant mice at day 12.5 of gestation, Cre-mediated recombination was induced and β-catenin was stabilized in embryos at E17.5 (Matsumoto et al., 2016). Compared with *Ctnnb1*$^{(Ex3)fl/fl}$ (control) embryos at E17.5, ppMLC, α18 and F-actin in adherens junctions and podocalyxin in the apical cortices of lung epithelium were clearly observed in *Ctnnb1*$^{(Ex3)fl/fl}$*;Cre* embryos as seen in control embryos at E14.5 (Fig. 2). The lung epithelium was composed of columnar-shaped cells in *Ctnnb1*$^{(Ex3)fl/fl}$*;Cre* embryos at E17.5, suggesting that downregulation of the β-catenin pathway is required for cell shape change and for apical cytoskeletal reorganization during the transition from the pseudoglandular to the canalicular-saccular stages.

Whether the β-catenin pathway is required for bud formation was examined using lung rudiments from E11.5 and mesenchyme-free epithelium from the same lung rudiments. Whereas the epithelium in control lung rudiments formed multiple buds during a 3-day culture, treatment with XAV939, an inhibitor of the β-catenin pathway that possibly affects cell proliferation (Goss et al., 2009), reduced the distal bud number (Fig. 3A,B). XAV939 treatment did indeed decrease the mRNA level of the β-catenin pathway target *Axin2*, but had no impact on epithelial cell proliferation during the culture period (Fig. S2A,B). This suggests that decreased bud formation by inhibition of the β-catenin pathway is not caused by the loss of proliferative activity.

To examine whether the β-catenin pathway can induce epithelial bud formation, mesenchyme-free epithelium isolated from E11 lung rudiments was embedded in Matrigel and cultured in the presence of FGF10 (Nogawa and Ito, 1995). In the presence of 200 ng/ml FGF10 (low FGF10), the lung epithelium initially formed buds within 2 days and then lost new bud formation activity (Fig. 3C). When the lung epithelium was cultured with low FGF10 and 1 μM CHIR99021 (FGF10-CHIR), an agonist of the β-catenin pathway, uniformly sized buds (ranging from 80 to 160 μm) were continuously induced during 4-day culture (Fig. 3C,D). Taken together, these results suggest the ability of the β-catenin pathway to induce bud formation.

It has been reported that the β-catenin pathway is involved in the proximal-distal specification of lung epithelium by suppressing the expression of *Sox2*, a proximal airway marker (Hashimoto et al., 2012; Miller et al., 2012). In lung epithelium culture, CHIR99021 treatment decreased and increased mRNA levels of *Sox2* and the distal progenitor marker *SOX9* (Chang et al., 2013), respectively (Fig. S2C). This suggests that the morphological differences between lung epithelium cultured with low FGF10 and FGF10-CHIR are due to different cell type composition, the former being composed of proximal and the latter of distal airway epithelial cells. The β-catenin pathway upregulates FGF signaling during lung development by inducing expression of FGF receptors (FGFRs) such as FGFR2 and 4 (Shu et al., 2005) (Fig. S2E), raising the possibility that the effect of CHIR99021 on bud formation might be caused by distal progenitor maintenance through the upregulation of FGF signaling. To test this hypothesis, lung epithelium was treated with 500 ng/ml FGF10 (high FGF10). Whereas only *Axin2* was upregulated in lung epithelium cultured with FGF10-CHIR, *Sox2* and *Sox9* mRNA levels were decreased and increased, respectively, in epithelium cultured with high FGF10 compared with low FGF10 (Fig. S2C). SOX9-positive cells were localized to the tips of buds in lung epithelium cultured with either high FGF10 or FGF10-CHIR (Fig. S2D), indicating that distal progenitors are maintained in both cultures. However, the number of buds in the lung epithelium cultured with high FGF10 was decreased compared with FGF10-CHIR (Fig. 3B,C), and various sized buds (ranging from 40 μm to 280 μm) emerged during 3- to 4-day culture (Fig. 3C,D). Therefore, these data suggest that, in addition to progenitor maintenance, the activation of the β-catenin pathway results in a gain-of-function ability to complement bud formation.

Whether the β-catenin pathway is required for the apical cytoskeletal organization of lung epithelium was then examined. Podocalyxin was only observed at the apical surface in the epithelium of lung rudiments (Fig. 3E). In XAV939-treated rudiments, podocalyxin in the epithelium was not only distributed at the apical surface, but was also observed in the cytosol and lateral membrane, suggesting loss of apical cytoskeletal organization (Fig. 3E). The distribution of ezrin, a marker of the apical cytoskeleton and podocalyxin binding partner (Bryant et al., 2014), in XAV939-treated lung rudiments was clearly shifted to the basal and lateral membrane (Fig. 3E). In mesenchyme-free epithelium culture, podocalyxin, ezrin and aPKCζ, a marker of apical-basal polarity, were localized at the apical surface in the presence of FGF10-CHIR, whereas apical distribution of podocalyxin, ezrin and aPKCζ was impaired and these proteins were observed in the basal and lateral membranes of the epithelium

Development (2017) 144, 151-162 doi:10.1242/dev.141325

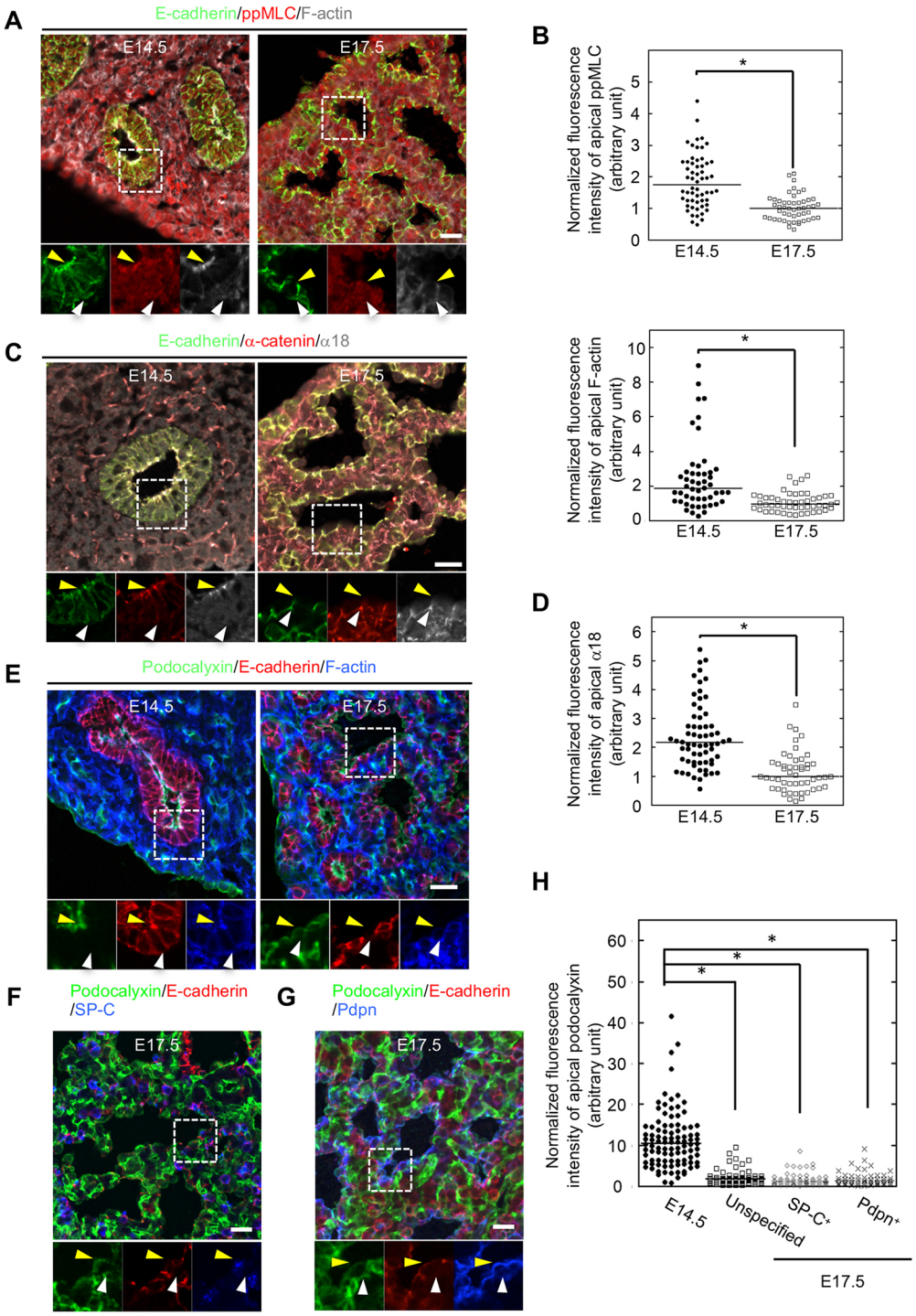

Fig. 1. Apical cytoskeletal organization in the pseudoglandular (E14.5) and canalicular-saccular (E17.5) stages. (A) Frozen sections from embryonic lungs at E14.5 and E17.5 were stained with anti-E-cadherin (green) and anti-ppMLC (red) antibodies, and phalloidin (gray). Yellow and white arrowheads indicate the edge of apical and basal junctions, respectively. (B) Fluorescence intensities of ppMLC (top) and F-actin (bottom) localized at the edge of apical junctions, as shown in A, were normalized to that of basal junctions. The ratio is shown as arbitrary units. (C) Frozen sections from embryonic lungs at E14.5 and E17.5 were stained with anti-E-cadherin (green), anti-α-catenin (red) and α18 (gray) antibodies. Yellow and white arrowheads indicate the edge of apical and basal junctions, respectively. (D) Fluorescence intensities of α18 localized at the edge of apical junctions, as shown in C, were normalized to that of basal junctions. The ratio is shown as arbitrary units. (E) Frozen sections from embryonic lungs at E14.5 and E17.5 were stained with anti-Pdpn (green) and anti-E-cadherin (red) antibodies, and phalloidin (blue). Yellow and white arrowheads indicate the midpoint of apical and basal cortices, respectively. (F,G) Frozen sections from embryonic lungs at E17.5 were stained with anti-podocalyxin (green), anti-E-cadherin (red) and anti-SP-C (blue) antibodies (F); or with anti-podocalyxin (green), anti-E-cadherin (red) and anti-Pdpn (blue) antibodies (G). Yellow and white arrowheads indicate the midpoint of the apical and basal cortices, respectively. (H) Fluorescence intensities of podocalyxin localized at the midpoint of the apical cortices, as shown in E-G, normalized to that of the basal cortices were plotted and shown as arbitrary units. Unspecified, cell types that were not specified; SP-C$^+$, SP-C-positive type II cells; Pdpn$^+$, Pdpn-positive type I pneumocyte. The horizontal bars in B,D,H indicate median values for each plot. *P<0.0001 (Mann–Whitney U-test). Insets in A,C,E,F are enlargements of the boxed areas above. Scale bars: 20 µm.

Development (2017) 144, 151-162 doi:10.1242/dev.141325

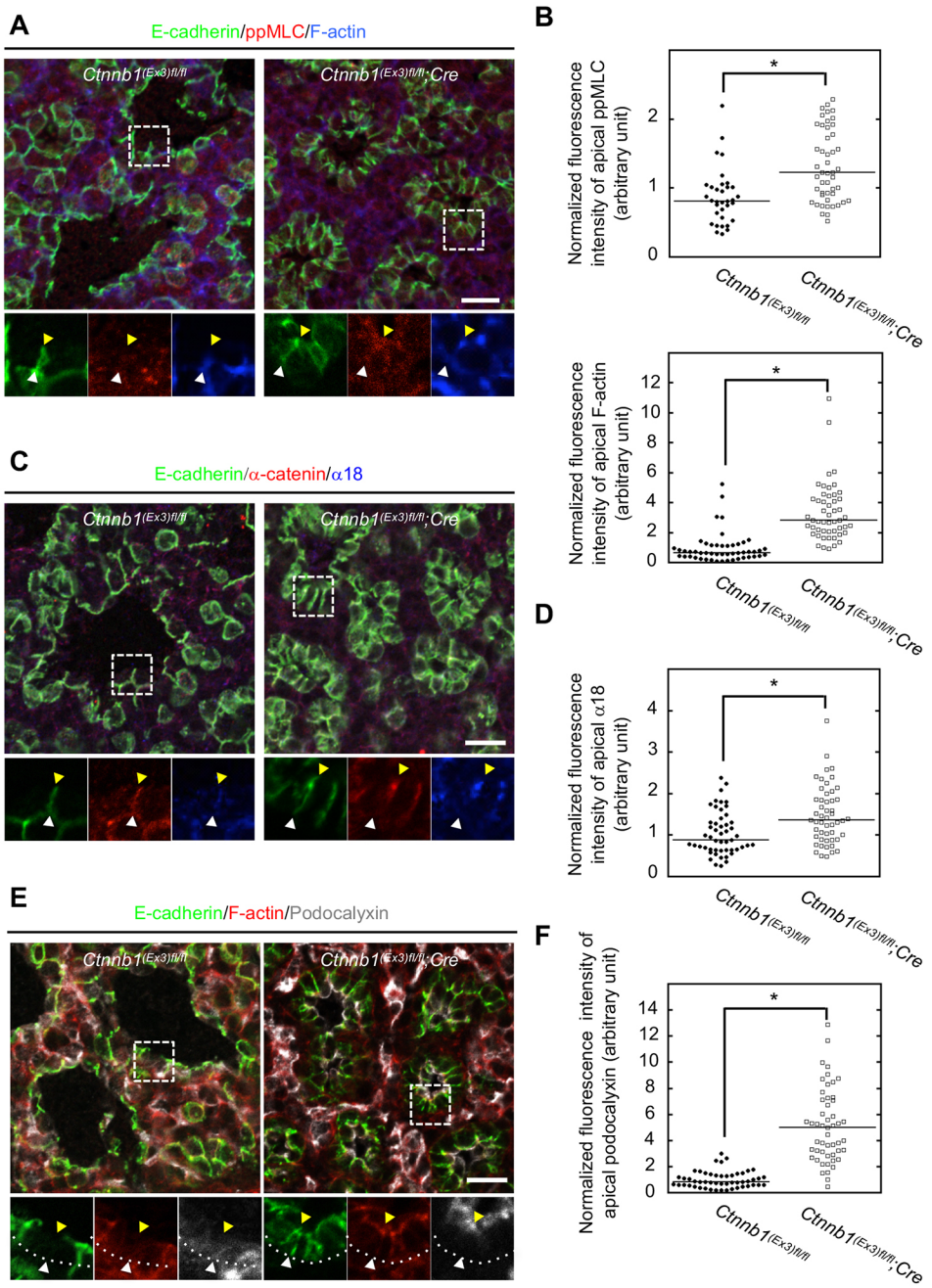

Fig. 2. Activation of β-catenin pathway *in vivo* sustained the apical cytoskeleton. (A) Frozen sections from control and *Ctnnb1*$^{(Ex3)fl/fl}$*;Cre* embryonic lungs at E17.5 were stained with anti-E-cadherin (green) and anti-ppMLC (red) antibodies, and phalloidin (blue). Yellow and white arrowheads indicate the edge of apical and basal junctions, respectively. (B) Fluorescence intensities of ppMLC (top) and F-actin (bottom) localized at the edge of apical junctions, as shown in A, were normalized to that of basal junctions. The ratio is shown as arbitrary units. (C) Frozen sections from control and *Ctnnb1*$^{(Ex3)fl/fl}$*;Cre* embryonic lungs at E17.5 were stained with anti-E-cadherin (green), anti-α-catenin (red) and α18 (blue) antibodies. Yellow and white arrowheads indicate the edge of apical and basal junctions, respectively. (D) Fluorescence intensities of α18 localized at the edge of apical junctions, as shown in C, were normalized to that of basal junctions. The ratio is shown as arbitrary units. (E) Frozen sections from control and *Ctnnb1*$^{(Ex3)fl/fl}$*;Cre* embryonic lungs at E17.5 were stained with anti-podocalyxin (gray) and anti-E-cadherin (green) antibodies, and phalloidin (red). Yellow and white arrowheads indicate the midpoint of apical and basal cortices, respectively. Dotted lines indicate basal membrane. (F) Fluorescence intensities of podocalyxin localized at the midpoint of apical cortices, as shown in E, normalized to that of basal cortices were plotted and shown as arbitrary units. The horizontal bars in B,D,F indicate median values for each plot. *P<0.0001 (Mann–Whitney U-test). Insets in A,C,E are enlargements of the boxed areas above. Scale bars: 20 µm.

cultured with low or high FGF10 (Fig. 3F). Taken together, these results suggest that the β-catenin pathway is necessary and sufficient for the induction of epithelial bud formation and apical cytoskeletal organization and, without it, bud morphology results in the loss of a uniform shape.

To obtain insight into the relationship between apical cytoskeletal organization and lung epithelial cell shape in the pseudoglandular and canalicular-saccular stages, the differentiation ability of cultured epithelium was examined. For this purpose, the tips of buds, which contain five to eight buds, were cut from primary lung epithelium (passage 0, P0) cultured with FGF10-CHIR, and re-embedded in Matrigel (P1). As observed in P0 epithelium, P1 lung epithelium also showed bud formation when cultured with FGF10-CHIR but not with low FGF10 (Fig. S3A). When distal airway markers expressed during the pseudoglandular stage (Desai et al., 2014; Treutlein et al., 2014) were examined, *Sox11*, another distal progenitor marker, and *Sox9* were expressed in CHIR99021-treated P0 and P1 lung epithelium cultures, and *Sox9* was increased in response to CHIR99021 more efficiently in P1 than in P0 culture (Fig. S3B). Although *SP-C* was concomitantly expressed in CHIR99021-treated lung epithelium compared with low FGF10 (Fig. S3B,C), *SP-C* is known to be expressed from the pseudoglandular stage (Treutlein et al., 2014) and CHIR99021-treated lung epithelium did not express *SP-B* or *Abca3*, mature type II pneumocyte markers (Desai et al., 2014; Treutlein et al., 2014). These data suggest that CHIR99021-treated lung epithelium is maintained in a distal progenitor state as seen during the pseudoglandular stage.

Interestingly, P1 lung epithelium cultured with low FGF10 expressed Pdpn at a higher level than CHIR99021-treated lung epithelium, suggesting that P1 epithelium cultured with low FGF10 is differentiated as observed during the canalicular-saccular stages (Fig.

Development (2017) 144, 151-162 doi:10.1242/dev.141325

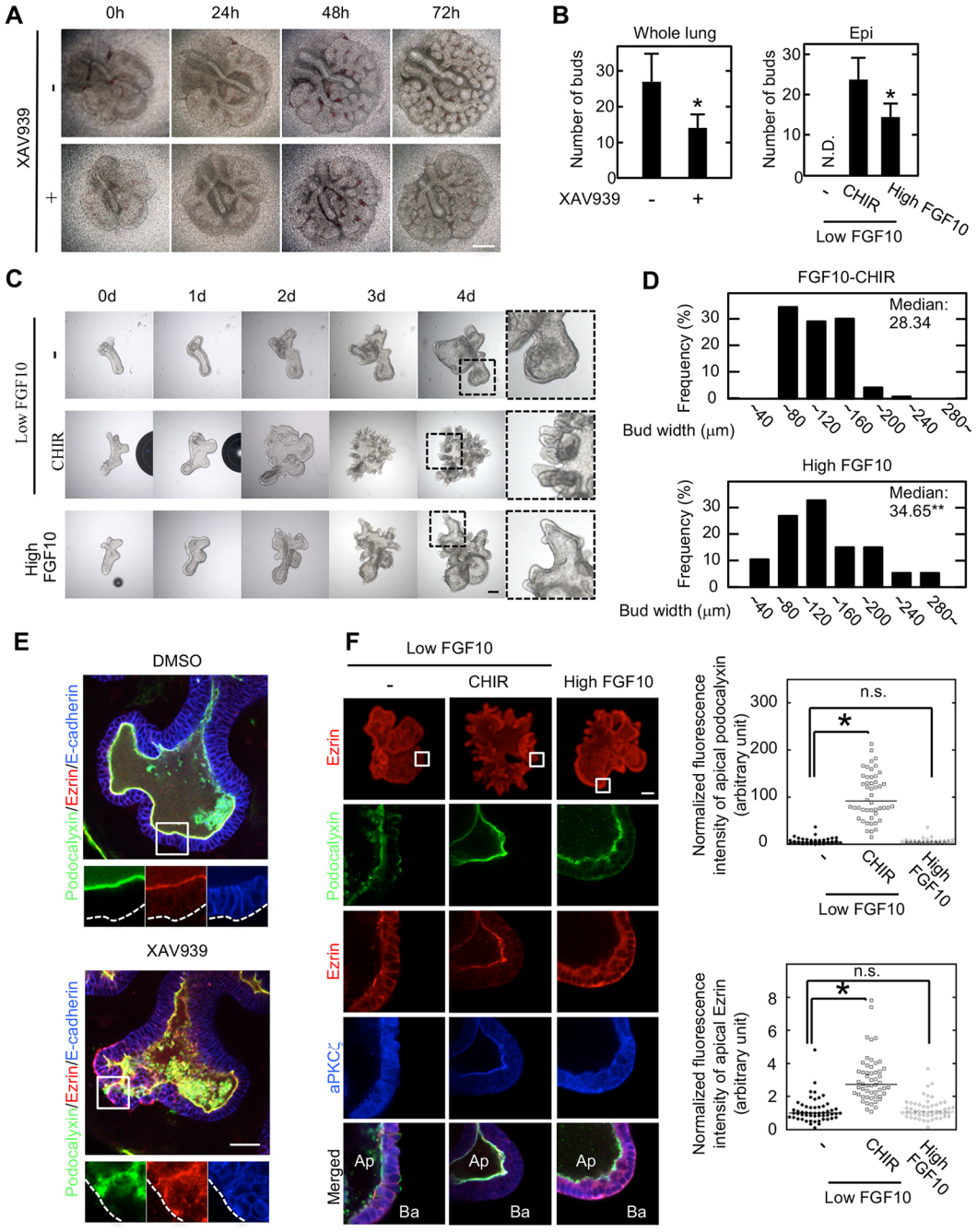

Fig. 3. Effect of the β-catenin pathway on bud formation and the apical cytoskeleton. (A) Whole lung rudiments treated with or without 5 µM XAV939 were cultured for the indicated period of time. (B) The number of distal tips of the lung rudiments shown in A (left, whole lung) and of the mesenchyme-free lung epithelium shown in C (right, epi) were quantified. Error bars indicate s.d. **P*<0.01 (Student's *t*-test). N.D., not determined. (C) Mesenchyme-free lung epithelium was embedded in Matrigel and cultured in serum-free medium containing 200 ng/ml (low) or 500 ng/ml (high) FGF10 in the presence or absence of 1 µM CHIR99021. (D) The width of buds in the mesenchyme-free lung epithelium cultured with high FGF10 or with 200 ng/ml FGF10 in the presence of 1 µM CHIR99021 (FGF10-CHIR) was measured and shown as a frequency histogram. ***P*<0.05 (Mann–Whitney U-test). (E) Whole lung rudiments were treated with or without 5 µM XAV939 and stained with anti-podcalyxin (green), anti-ezrin (red) and anti-E-cadherin (blue) antibodies. Typical branches are shown and the boxed areas are enlarged below. (F) Left: mesenchyme-free lung epithelium cultured with low FGF10, FGF10-CHIR or high FGF10 was stained with anti-podcalyxin (green), anti-ezrin (red) and anti-atypical PKC (aPKC, blue) antibodies. Boxed areas in the top panels are enlarged below. Ap, apical; Ba, basal. Right: fluorescence intensities of podocalyxin (top) and ezrin (bottom) localized at the midpoint of apical cortices as shown in left panels normalized to that of basal cortices were plotted and shown as arbitrary units. Horizontal bars indicate median values for each plot. **P*<0.0001 (Mann–Whitney U-test). n.s., not significant. Scale bars: 100 µm (A,F); 200 µm (C); 50 µm (E).

S3B,C). Microarray analysis in which P1 lung epithelium cultured with FGF10 was compared with that cultured with FGF10-CHIR showed that the former expresses type I and II pneumocyte-enriched genes and the latter expresses few pneumocyte markers (Fig. S3D). These data suggest that P1 lung epithelium cultured with FGF10-CHIR mimics progenitor cells in the distal end of the pseudoglandular stage and that cultured with low FGF10 mimics pneumocytes during the canalicular-saccular stages more efficiently

Development (2017) 144, 151-162 doi:10.1242/dev.141325

than P0 epithelium. From these observations, P1 lung epithelium was used in subsequent experiments (Fig. 4; Fig. S4) to analyze the effect of the β-catenin pathway on epithelial cell shape changes during the pseudoglandular and canalicular-saccular stages.

Apically constricted cell shape is induced by the β-catenin pathway

The impact of apical formation by the β-catenin pathway on lung epithelial cell shape change was examined using P1 lung epithelium. When lung epithelial cells were observed from the lateral side, the cells at the bud tips were elongated along the apical-basal axis in a dose-dependent manner, but basal length was unchanged by CHIR99021 treatment in the presence of low FGF10 (Fig. 4A). When the apical cortex area was compared with that of the basolateral cortex, the apical cortex was constricted at the tip of buds in CHIR99021-treated lung epithelium (Fig. 4B,C). Apical constriction was partially relieved by treatment with Y27632, a Rho-kinase inhibitor (Fig. 4B,C). These data indicate that activation of the β-catenin pathway induces a laterally extended and apically constricted cell shape in the lung epithelium. Concomitantly, myosin locally accumulated at the apical membrane in CHIR99021-treated lung epithelium (Fig. 4D). Vinculin is an actin-binding protein known to be recruited to adherens junctions when the conformation of α-catenin is changed by actomyosin-mediated pulling forces (Yonemura et al., 2010). Vinculin was clearly detected at both the apical membrane and cell-cell junctions after CHIR99021 treatment (Fig. 4D). Thus, apical actomyosin contractility is locally increased by CHIR99021 treatment, resulting in the induction of apical constriction as seen at the pseudoglandular stage. Conversely, both myosin and vinculin decreased in the apical membrane in the absence of CHIR99021 as seen at the canalicular-saccular stages.

When lentivirus harboring Wnt2 was transduced into P0 lung epithelium to examine the effects of the β-catenin pathway on P1 lung epithelium, bud formation was induced in the absence of CHIR99021, and Sox9 expression was maintained (Fig. S4A-C). Wnt2 expression also induced recruitment of podocalyxin to the apical membrane and constriction of the apical cortex, as was seen in lung epithelium cultured with FGF10-CHIR (Fig. S4D,E). Taken together, the CHIR99021-treated lung epithelial model represents the functional roles of the β-catenin pathway in apical cytoskeletal organization as seen in the pseudoglandular stage although the possibility that CHIR99021 might induce off-target effects cannot be excluded.

Mathematical modeling shows that self-organized epithelial morphogenesis depends on apical constriction and outward movement of epithelial cells

To examine how cellular morphological changes induced by apical constriction affect lung epithelial tissue shape, a mathematical model of the abstract mechanical interaction between the cells of an epithelial cyst in two-dimensional space was developed. Without losing generality, we adapted a two-dimensional model by considering the shape of the cyst in cross-section. The cell was represented by four vertices that are shared between adjacent cells (Fig. 5A). Cell shape change, movement and division were described by the movements and addition of vertices in the model. The possible effect of cell deformation accompanied by cell division on tissue morphology was omitted from the model, and the basic assumption that daughter cells evenly take over the area of mother cells was adopted (Fig. 5B). Cells are considered to exert an elastic restoring force to maintain cell appearance (Luu et al., 2011; Nagai and Honda, 2001). Vertices were assumed to move to maintain the length of the basal edge and cell perimeter based on our morphometric results (Fig. 4A-C). Apical constriction was described as attractive forces between adjacent vertices on the apical side, which eventually lengthen the lateral edge (Fig. 5C). In this study, the simplest assumption was adopted that the cellular property involved in regulating cell appearance, including apical constriction, is homogeneous throughout the cyst.

The tissue growth process, including progressive apical constriction, was described using the model framework (Fig. 5D; Movie 1). Computer simulation demonstrated that the cyst gradually develops uniformly sized buds composed of thickened cells. Despite the assumption that all cells exert constriction forces, buds and clefts spontaneously emerged. Although cells under apical constriction preferentially took a wedge-like shape, cell shapes were necessarily less wedged as the global curvature of the cyst was decreased by tissue growth. Mechanical instability occurs when the total energy of the deformed morphology is favorable compared with that of evenly rounded tissue. As a result, cells at clefts showed elongated apical sides to maximize highly curved regions within the cyst. The characteristic bud size (i.e. the wavelength of epithelial folds) depended on the spontaneous curvature of the wedge-like shape of the cell, which is determined by the collective mechanics between identical cells. This result was expected to be extended to three dimensions (Auth and Gompper, 2009). It was confirmed that uniformly sized buds are not induced when the magnitude of apical constriction is reduced, suggesting that apical constriction is required for reproducing regular bud formation as observed (Fig. 5E; Movie 2).

The effect of relaxation of apical constriction, as occurs in the canalicular-saccular stages, on cyst morphology was examined. Because the number of dividing cells was significantly reduced in E17.5 lung epithelium (Fig. S5), the proliferation rate was also decreased after the reduction of apical constriction in the model. It was revealed that buds fail to unfold after apical constriction decay, though cells became thinner and their shapes were slightly smoothened (Fig. 5F; Movie 3). Growth factor signaling mediates both proliferation and outward movement of lung epithelium (Morrisey and Hogan, 2010; Weaver et al., 2000). The force pulling basal vertices in directions perpendicular to the basal ridge was introduced throughout the course of elevation and reduction of apical constriction (Fig. 5H; Movie 4). Bud unfolding, as seen in air sac-like structure formation, was successfully reproduced. We confirmed that unfolding fails when apical constriction is sustained (Fig. 5I; Movie 5). These results imply that lowered apical constriction in the presence of outward movement is required for air sac formation.

To evaluate whether the effects of the β-catenin pathway on the apical cytoskeleton and cell shape are cell-autonomous, adenomatous polyposis coli (Apc), a negative regulator of the Wnt pathway, was depleted in the lung epithelium to activate the β-catenin pathway in a mosaic fashion. An active (non-phosphorylated) form of β-catenin was detected in a mosaic fashion and ezrin was accumulated at the apical cortex of epithelial cells compared with the surrounding cells where β-catenin was not detected (Fig. S6A,B), suggesting that activation of the β-catenin pathway induces apical cytoskeletal organization in a cell-autonomous manner. However, local deformation of the cells in which the β-catenin pathway is activated was not observed, and the mathematical model suggested that the result of the mosaic experiment depends on the balance between the force for apical constriction and neighboring cell shapes (Fig. S6C).

Development (2017) 144, 151-162 doi:10.1242/dev.141325

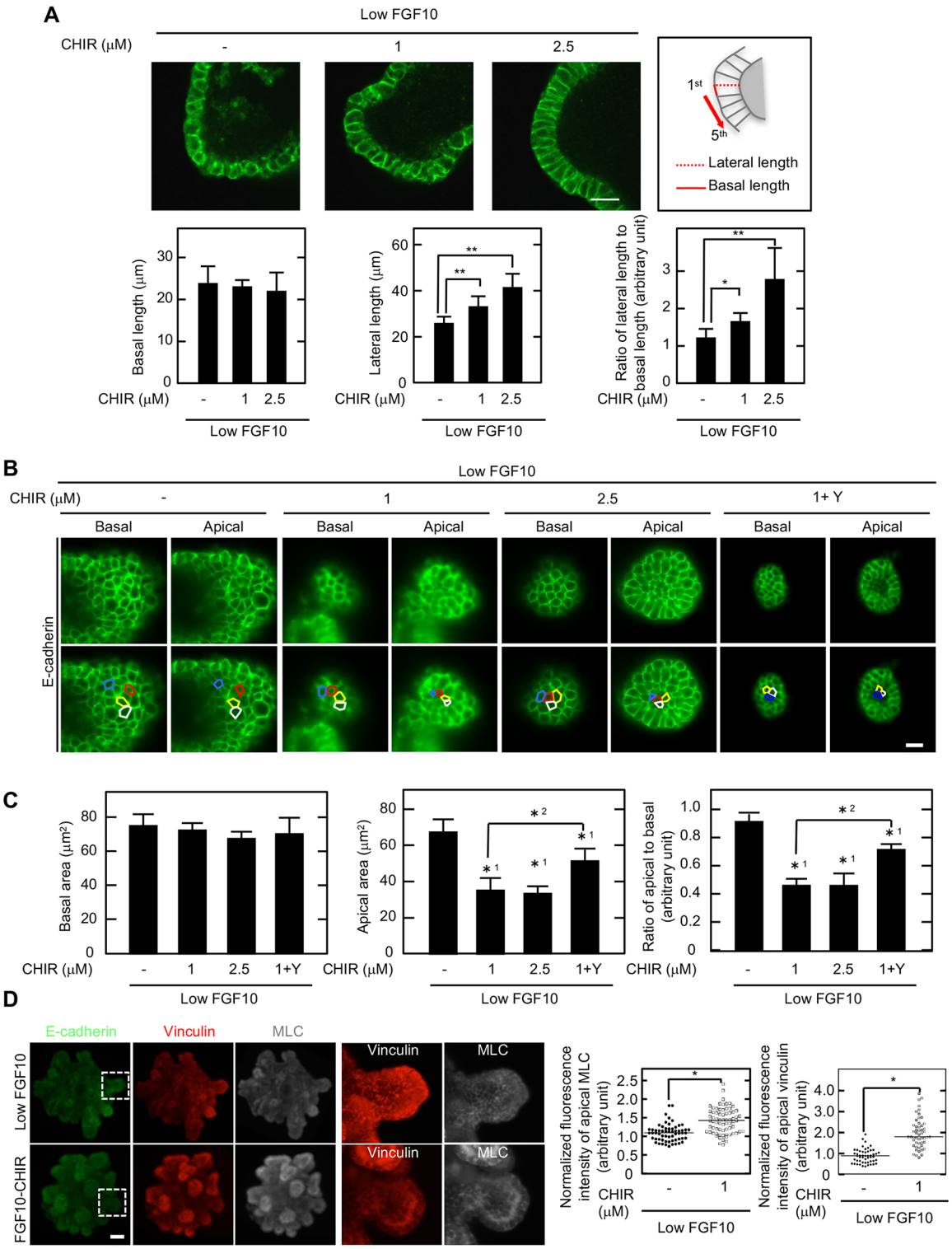

Fig. 4. Impact of the β-catenin pathway on cell shape change and apical constriction. (A) Top left: mesenchyme-free P1 lung epithelium cultured with low FGF10 in the presence of 1 or 2.5 µM CHIR99021 was stained for E-cadherin. Top right: epithelial cells that are positioned at the tips of buds were numbered as first to fifth from the vertices. Bottom: the length of the basal (red lines in schematic) and lateral (red dotted lines in schematic) cortices of individual cells was measured and those from the first to fifth cells were averaged. The ratios of lateral to basal lengths of individual cells were calculated and those from the first to fifth cells were averaged. Results are shown as mean±s.d. **P*<0.05; ***P*<0.01. (B,C) Mesenchyme-free P1 lung epithelium cultured with low FGF10 in the presence or absence of 1 or 2.5 µM CHIR99021 and 10 µM Y27632 (Y) was stained with anti-E-cadherin antibody (B, top) and apical and basal cortices of individual cells positioned at the tips of buds are encircled (B, bottom). Apical and basal areas were measured and are shown as mean±s.d. (C). **P*<0.05 (Student's *t*-test). *[1] or *[2] indicates the comparison of low FGF10 or FGF10-CHIR with Y27632, respectively. (D) Left: mesenchyme-free P1 lung epithelium cultured with low FGF10 or FGF10-CHIR was stained with anti-E-cadherin (green), anti-vinculin (red) and anti-MLC (gray) antibodies. Right: fluorescence intensities of MLC and vinculin localized at the edge of apical junctions were normalized with that of basal junctions and are shown as arbitrary units. Horizontal bars indicate median values for each plot. **P*<0.0001 (Mann–Whitney U-test). Scale bars: 20 µm (A); 100 µm (D).

Development (2017) 144, 151-162 doi:10.1242/dev.141325

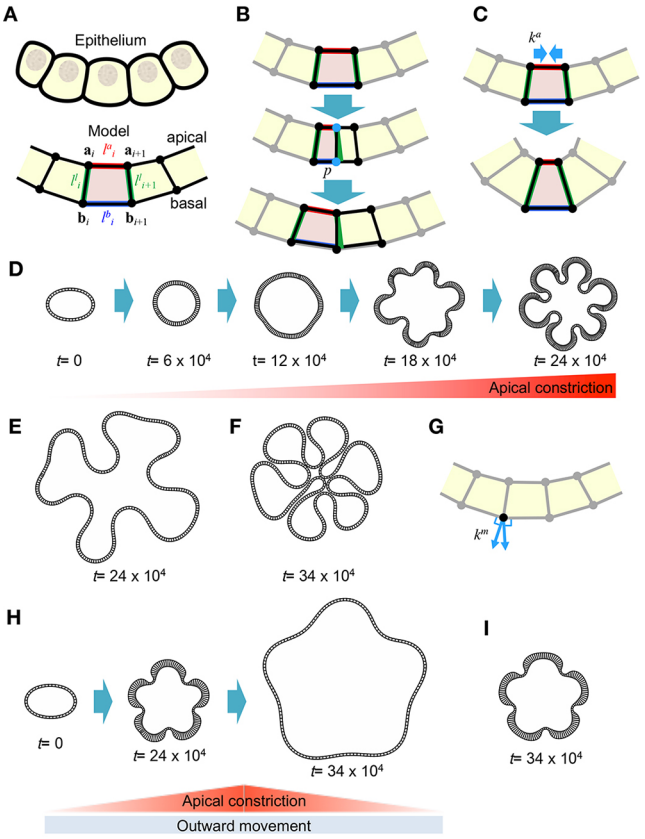

Fig. 5. Mathematical modeling of epithelial shape change through apical constriction. (A) The lung epithelium was described as a sequence of tetragons in the model. The *i*-th cell was represented by vertices the positions of which are denoted by $\mathbf{a}_i$, $\mathbf{a}_{i+1}$, $\mathbf{b}_i$ and $\mathbf{b}_{i+1}$. It was assumed that l_i^a was controlled by apical constriction. The cell was assumed to exert an elastic restoring force to maintain l_i^b and perimeter ($l_i^a + l_i^b + l_i^l + l_{i+1}^l$ where l_i^a is apical length, l_i^b basal length and l_i^l lateral length). (B) Cell division was described by inserting new vertices to the middles of the edges at a probability p for fully grown cells and the perimeters of the daughter cells were reduced accordingly. Daughter cells were assumed to grow gradually over 5000 time steps to become fully grown cells. (C) Apical constriction was defined as the attraction of the apical vertices of a cell. The degree of apical constriction was defined by the value of k^a. (D) Snapshots at time steps t=0, 6×10^4, 12×10^4, 18×10^4 and 24×10^4 are shown. Cell division probability was set as p=1.2×10^{-5}. The degree of apical constriction was set as k^a=5 initially, and increased by 0.0012 at each time step to k^a=293. The cell number changed from 40 (t=0) to 272 (t=24×10^4). (E) The corresponding calculation to that described in D was performed, but with k^a=5 throughout. A snapshot at t=24×10^4 is shown. (F) After the process shown in D, the value for k^a was reduced by 0.0035 at each time step until k^a reached 0.5 and cell division probability was set at p=1.2×10^{-6} for an additional 12×10^4 time steps. A snapshot at time step t=34×10^4 is shown and the cell number is 306. (G) Basal vertices were assumed to move radially, and the extent of outward movement was defined as k^m=1. (H) Snapshots at time steps t=0, 24×10^4 and 34×10^4 are shown. Cell division probability was set at p=0.8×10^{-5} until t=24×10^4, and p=0.8×10^{-6} afterwards. The degree of apical constriction was set as k^a=5 initially, increased by 0.0012 at each time step to k^a=293 until t=24×10^4, and reduced by 0.0035 until k^a reached 0.5. The number of cells increased from 40 (t=0) to 147 (t=24×10^4) and 153 (t=34×10^4). (I) The corresponding calculation to that described in H was performed, but k^a=293 was sustained after t=24×10^4. A snapshot at time step t=34×10^4 is shown.

Mark1 is induced in lung epithelium downstream of the β-catenin pathway

To identify the molecular mechanism underlying Wnt-driven apical cytoskeletal organization, possible candidates were interrogated from the microarray data that was used to generate Fig. S3D. Among the genes increased by CHIR99021 treatment, we focused on MAP/microtubule affinity-regulating kinase 1 (Mark1). Mark1 is a Mark2/Par1b homolog, and Mark2 is a multifunctional kinase that directly or indirectly phosphorylates various substrates including cytoskeleton-associated proteins, such as MAPs and myosin, and the regulator of epithelial polarity Par-3 (Pard3), thereby regulating columnar epithelial cell shape (Böhm et al., 1997; McDonald, 2014). Mark1 was expressed in both lung epithelium and mesenchyme at E14.5 and, interestingly, it was distributed in the apical cytoplasm and in apical junctions in the epithelium (Fig. 6A, B). In the E17.5 lung, Mark1 expression in the mesenchyme was still observed, but the expression was decreased in the epithelium (Fig. 6A,B). When *Mark1* shRNA was introduced into the lung epithelium, the fluorescence intensity of apically localized Mark1 staining was decreased (Fig. S7A). The expression level of *Mark1* mRNA was higher in the periphery of the E14.5 lung compared with that of the E18.5 lung (Fig. 6C). *Mark1* mRNA expression was induced by CHIR99021 treatment in a dose-dependent manner in the presence of low FGF10, but FGF10 alone up to 2000 ng/ml did not affect *Mark1* mRNA levels (Fig. 6D). *Mark1* mRNA was increased when the lung epithelium was infected with lentivirus harboring Wnt2 or a constitutively activated form of β-catenin (Fig. 6D). By contrast, *Mark1* mRNA was decreased when lung rudiments were treated with XAV939 (Fig. 6D). A chromatin immunoprecipitation (ChIP) assay using E13.5 lung rudiments showed that β-catenin is recruited to the predicted Tcf/LEF1 binding region in the 5′-untranslated region of *Mark1* (Fig. 6E). These data suggest that *Mark1* is a possible downstream target of the β-catenin pathway during the pseudoglandular stage.

Mark1 is involved in apical cytoskeleton organization

When the lung epithelium was infected with lentivirus harboring *Mark1* shRNA, the bud number was reduced and irregularly sized buds were generated (Fig. 7A-C; Fig. S7B-D). Apical localization of ZO-1 (Tjp1), a tight junction marker, was redistributed to the basal side in *Mark1*-depleted lung epithelium despite the presence of CHIR99021 (Fig. 7D), indicating that cell height was partly shortened (see supplementary Materials and Methods). Ezrin was observed in the basal side of the *Mark1*-depleted lung epithelium despite the presence of CHIR99021 (Fig. 7E; Fig. S7E). Myosin was not localized apically in *Mark1*-depleted lung epithelium (Fig. 7F). These results suggest that Mark1 is involved in apical cytoskeleton organization downstream of the β-catenin pathway during lung epithelial bud formation.

DISCUSSION

Although it is well known that cellular morphology drastically changes during the transition from the pseudoglandular to the saccular stages of lung development, the impact of cell shape change on tissue morphological changes has not been adequately addressed. Here, we showed that modulation of Wnt activity has a differential impact on epithelial cell shape through apical cytoskeletal reorganization, leading to tissue morphological changes. The expression levels of Wnt ligand and Wnt signaling molecules were decreased in the canalicular-saccular stages, and genetically constitutive activation of the β-catenin pathway impaired apical cytoskeletal reorganization *in vivo*. In cultured embryonic lungs, the β-catenin pathway was required for the apical cytoskeletal organization and uniformly sized bud formation. As ectopic activation of the β-catenin pathway in fetal lung expands Sox9-expressing epithelial cells (Hashimoto et al., 2012), the

Development (2017) 144, 151-162 doi:10.1242/dev.141325

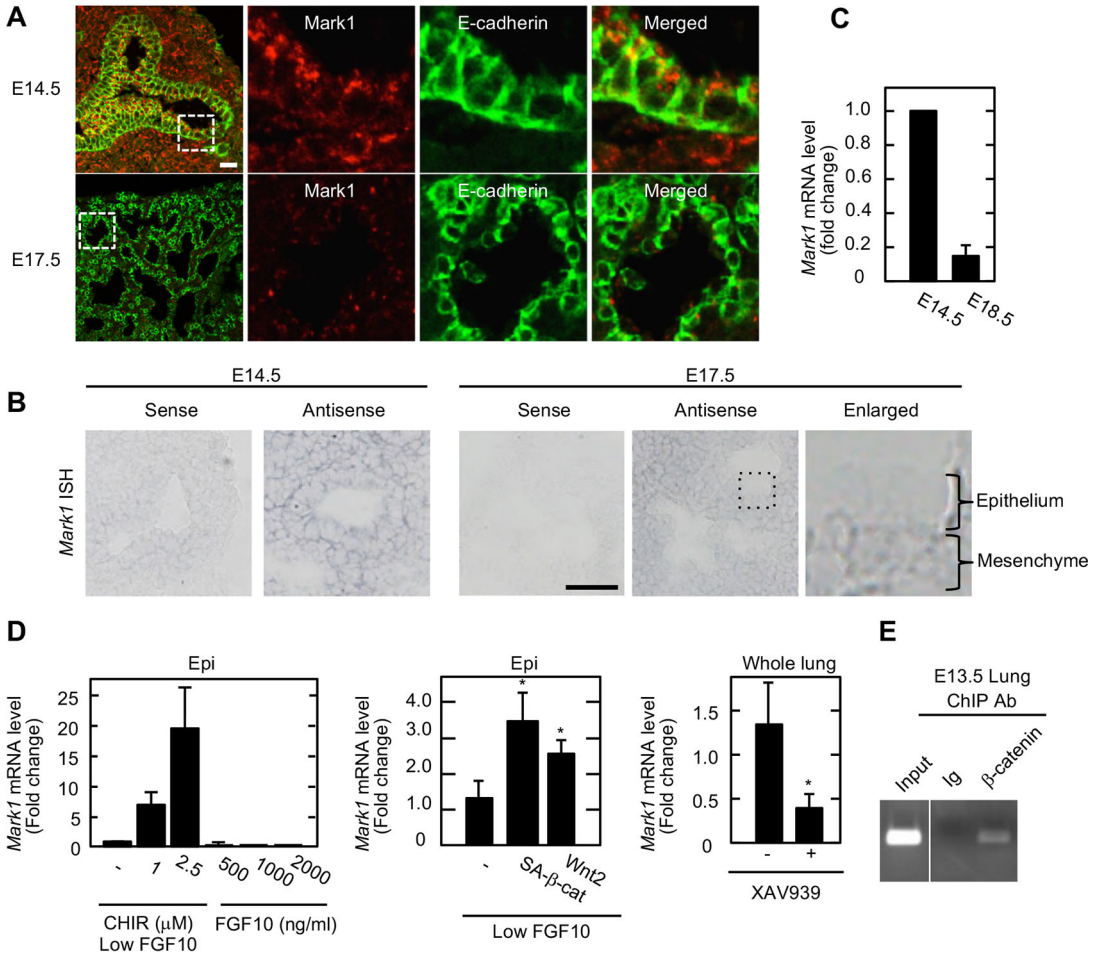

Fig. 6. Identification of Mark1 as a downstream target of the β-catenin pathway. (A) Frozen sections from embryonic lungs at E14.5 and E17.5 were stained with anti-Mark1 (red) and anti-E-cadherin (green) antibodies. (B) The expression of *Mark1* mRNA in frozen sections from E14.5 and E17.5 lungs was examined using *Mark1* sense and antisense RNA probes. The boxed region is enlarged on the right. (C) *Mark1* mRNA levels in embryonic lungs at E14.5 and E18.5 were measured by quantitative RT-PCR. Relative mRNA levels were normalized to *Actb* and are shown as fold changes compared with *Mark1* mRNA levels in the distal end of the E14.5 lung. (D) *Mark1* mRNA levels of mesenchyme-free lung epithelium (epi) and whole lung rudiments were measured by quantitative RT-PCR. Left: lung epithelium treated with the indicated concentration of CHIR99021 and FGF10. Middle: lung epithelium infected with SA-β-catenin- or Wnt2-harboring lentiviruses. Right: whole lung rudiments treated with or without XAV939. Results are expressed as fold changes compared with *Mark1* mRNA levels in controls. **P*<0.05 (Student's *t*-test). (E) A chromatin immunoprecipitation (ChIP) assay was performed using chromatin from E13.5 whole lungs and non-immune Ig or anti-β-catenin antibodies. Precipitates were analyzed by PCR with region-specific primers. Error bars represent s.d. Scale bars: 20 μm (A); 50 μm (B).

β-catenin pathway might induce bud formation through the expansion of the distal progenitors. However, our results revealed that apical cytoskeletal organization and uniformly sized buds are only induced by FGF10-CHIR but not by high FGF10, although high FGF10 induced *Sox9* expression to the same extent as FGF10-CHIR. We identified Mark1 as a downstream effector of the β-catenin pathway and showed that apical cytoskeletal organization was disrupted in *Mark1*-depleted lung epithelium cultured with FGF10-CHIR. Altogether, these results suggest that the β-catenin pathway regulates the apical cytoskeletal organization independently of distal progenitor maintenance.

Development of the actomyosin network in the apical membrane and adherens junctions is required for contractile force generation during apical constriction (Martin and Goldstein, 2014). We showed that the β-catenin pathway is required for apical constriction through apical cytoskeletal organization in the lung epithelium. Myosin is recruited apically by Mark1 downstream of the β-catenin pathway and force is generated apically. At present, the precise mechanism of apical cytoskeletal organization by Mark1 is unclear. As Mark proteins regulate microtubule stability (McDonald, 2014) and microtubule stability is involved in apical constriction (Fernandes et al., 2014; Lee and Harland, 2007), it is possible that organization of the microtubule array by Mark1 is involved in apical constriction. Mark proteins also indirectly regulate myosin activity. However, although MARKs activate myosin function in border cell migration during *Drosophila* development (Majumder et al., 2012), myosin activity is suppressed by Mark proteins during lumen polarity formation in MDCK cells (Lázaro-Diéguez et al., 2013). Direct substrates of Mark1 in the lung epithelium need to be identified in the future.

To examine the role of MARK1 *in vivo*, mutant animals were generated using the triple CRISPR method (Sunagawa et al., 2016). Synthesized Cas9 mRNA and guide RNAs (gRNAs) were microinjected into cytoplasm of B6C3F1 one-cell embryos (Fig. S8A). E14 embryos were obtained and they were all mutant animals as confirmed by quantitative PCR (Fig. S8B). Although shRNA-mediated Mark1 knockdown in the lung epithelium disrupted apical cytoskeleton, these mutant embryos did not exhibit obvious effects on epithelial morphology and the apical cytoskeletal organization (Fig. S8C). As it has been suggested that

Development (2017) 144, 151-162 doi:10.1242/dev.141325

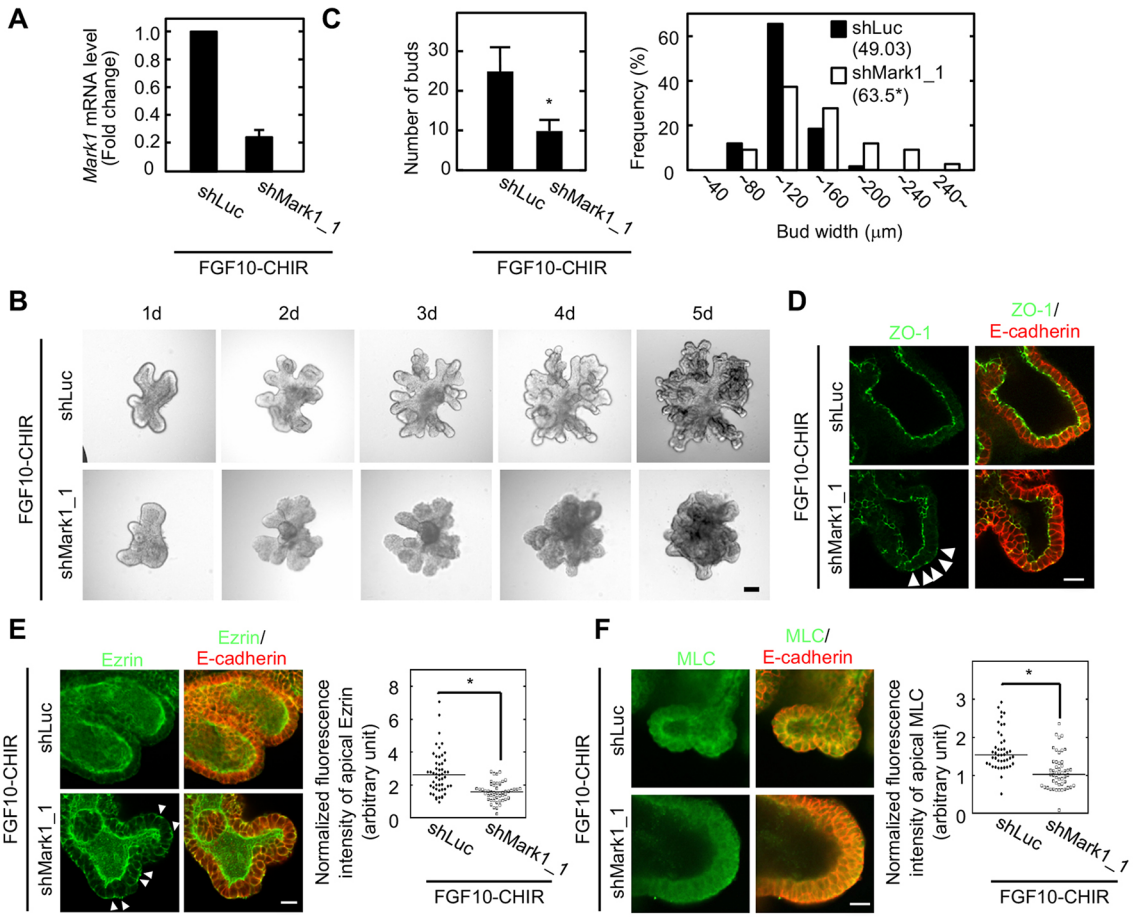

Fig. 7. Involvement of Mark1 in apical constriction and uniformly sized bud formation downstream of the β-catenin pathway. (A) The *Mark1* mRNA levels of mesenchyme-free lung epithelium infected with *Mark1* shRNA (shMark1_1) were measured by quantitative RT-PCR. Results are expressed as fold changes compared with the *Mark1* mRNA level in the lung epithelium treated with control shRNA. Error bars represent s.d. (B) Mesenchyme-free lung epithelium infected with shMark1_1 was cultured for 5 days in FGF10-CHIR. (C) Left: number of distal tips of shMark1_1-expressing mesenchyme-free lung epithelium was counted. **P*<0.01 (Student's *t*-test). Error bars represent s.d. Right: width of buds in shMark1_1-expressing mesenchyme-free lung epithelium cultured with FGF10-CHIR was measured and shown as a frequency histogram. (D-F) Mesenchyme-free lung epithelium infected with shMark1_1 was cultured with FGF10-CHIR and stained with anti-ZO-1 (green) and anti-E-cadherin (red) antibodies (D), with anti-ezrin (green) and anti-E-cadherin (red) antibodies (E), and with anti-MLC (green) and anti-E-cadherin (red) antibodies (F). Fluorescence intensities of Ezrin (E) and MLC (F) localized at the edge of apical junctions were normalized to those of basal junctions. The ratio is shown as arbitrary units. Horizontal bars indicate median values for each plot. **P*<0.0001 (Mann–Whitney U-test). shLuc, shRNA against luciferase. Scale bars: 100 μm (B); 20 μm (D-F).

genetic compensation can be induced by genome editing but not by knockdown (Rossi et al., 2015), the defect in Mark1 mutant embryos might have compensated for by other Mark family kinases, such as Mark2.

Our simulation model is novel in that it suggests the significance of apical contractility regulation in the switch from bud formation to sacculation. With growing attention to the concept of mechanical deformation to explain a variety of morphogenetic events (Ciarletta et al., 2014; Drasdo, 2000; Savin et al., 2011; Takigawa-Imamura et al., 2015; Varner et al., 2015), branching formation based on physical buckling (Varner et al., 2015) and local apical constriction (Kim et al., 2013) have been proposed as mechanisms of bud formation. In our model, apical constriction was assumed to occur globally within the cyst, and uniformly sized buds emerge spontaneously without pre-patterning of protruding regions. The same model also showed that by maintaining apical constriction, the air sac-like structure failed to form, suggesting that loss of apical constriction is necessary for air sac structure formation during the canalicular-saccular stages. However, cell flattening was not induced by XAV939 in whole lung rudiments. As the mathematical model showed, loss of apical constriction was not sufficient for air sac-like structure formation and an associated outward movement was required. In order to understand fully this observation, it will be necessary to identify the other signaling pathways that induce outward movement during the canalicular-saccular stages *in vivo*.

MATERIALS AND METHODS

Isolation and culture of embryonic lung rudiments and epithelium

Whole lung rudiments were isolated from 11.5-day-old ICR mice and placed on transwell filter supports (Corning). The lower chamber was filled with organ culture medium [DMEM:F12 (1:1) containing 0.1% bovine serum albumin (BSA), 75 ng/ml ascorbic acid (Nakarai, Kyoto, Japan) and 25 ng/ml transferrin (Thermo Fisher Scientific)]. For lung epithelium culture, lung epithelium from embryonic ICR mice was isolated and cultured as previously reported (Nogawa and Ito, 1995) with modifications. For further details, see supplementary Materials and Methods.

Mice

Protocols used for all animal experiments in this study were approved by the Animal Research Committee of Osaka University, Japan (No. 21-048-1).

Development (2017) 144, 151-162 doi:10.1242/dev.141325

All animal experiments were carried out according to Osaka University guidelines for the care and use of experimental animals. Tamoxifen administration in mice was performed as previously described (Matsumoto et al., 2016). *Mark1* mutant mice were generated using the triple CRISPR method as previously described (Sunagawa et al., 2016).

Lentivirus production and infection

Lentivirus production and infection was carried out as previously described (Fumoto et al., 2012) with modifications. For further details, see supplementary Materials and Methods.

In situ hybridization

For *in situ* hybridization, unfixed E14.5 or E17.5 lungs were frozen in OCT compound (Sakura Finetek, Tokyo, Japan). *Mark1* cDNA that was amplified using specific primers (forward: 5′-GTACCGCATCCCCTTCTACA-3′; reverse: 5′-GGCTGCTGTCTCTTCCATTC-3′), was cloned into the pCRII vector (Thermo Fisher Scientific). To generate RNA probes, digoxigenin-labeled antisense or sense RNA probes were synthesized with the DIG RNA Labeling Mix Kit (Sp6/T7; Roche Diagnostics). Ten-µm-thick sections were hybridized with RNA probes and incubated with anti-digoxigenin AP Fab fragments (Roche Diagnostics). Specific signals were visualized with BM-Purple (Sigma Aldrich).

Immunostaining

Freshly frozen embryonic lungs were sectioned at 18 µm, fixed in 4% paraformaldehyde (PFA) and blocked in blocking buffer (PBS containing 1% BSA and 0.3% Triton X-100). Samples were incubated with antibodies diluted in blocking buffer for 1 h or overnight, washed three times, and then stained overnight with secondary antibody diluted in blocking buffer. After washing, samples were covered with PBS containing 50% glycerol. Cultured lung epithelium was isolated from Matrigel using Cell Recovery Solution (BD Biosciences) and fixed with 4% PFA at room temperature for 30 min or 100% cold methanol at −20°C for 1 h. After blocking, the lung epithelium was stained as described above. All images were observed using a LSM880 and Lightsheet Z.1 (Carl Zeiss Microscopy). See supplementary Materials and Methods for details of antibodies.

EdU incorporation assay

EdU (5-ethynyl-2′-deoxyuridine) incorporation was performed using a Click-iT EdU Alexa555 Kit (Thermo Fisher Scientific). Whole lung rudiments were treated with EdU for 30 min. Proliferating lung epithelium was measured by quantifying the proportion of EdU-positive cells per total cells in the distal end.

Quantitative real-time PCR

Quantitative PCR was performed as previously described (Hino et al., 2005). Primers used for this analysis are summarized in Table S1.

Quantification of fluorescence intensity

Cell-cell junctions were visualized by E-cadherin (cadherin 1) and ezrin staining, and the fluorescence intensities of ppMLC, F-actin, α18, MLC and vinculin at the edge of apical and of basal junctions along the basolateral membrane (indicated by arrowheads in figures) were measured using ImageJ. For quantification of podocalyxin staining, the fluorescence intensities at the midpoint of the apical and basal cortices were measured. The fluorescence intensities of apical side were divided by that of the basal side. Normalized fluorescence intensities are expressed as arbitrary units.

Model description

The mechanical model of a cyst composed of a single layer of epithelial cells in two-dimensional space was constructed. For further details, see supplementary Materials and Methods.

Microarray analysis

Microarray analyses were performed using P1 lung epithelium cultured with low FGF10 and FGF10-CHIR. The mRNA expression profile was produced by Bio Matrix Research (Chiba, Japan) using gene microarray technology (GeneChip Affymetrix.GeneChip.Mouse430_2, Affymetrix, Santa Clara, CA, USA). After data analysis, the log fold change between the hybridization intensities of low FGF10 and FGF10-CHIR was determined. The data reported in this article have been deposited in NCBI GEO under accession number GSE83391.

Chromatin immunoprecipitation (ChIP) assay

E13.5 ICR lung rudiments were used in a ChIP assay. For further details, see supplementary Materials and Methods.

Statistical analysis

Experiments were performed at least three times and results are expressed as mean or mean±s.d. Statistical analysis was performed using a paired Student's *t*-test and Mann–Whitney U-test. For each quantification, at least 50 cells from at least three sections or lung epithelia were counted per experiment. *P*-values less than 0.05 were considered statistically significant.

Acknowledgements

We thank the Center of Medical Research and Education, Graduate School of Medicine, Osaka University for observation using Lightsheet Z.1. We would also like to thank Dr H. Miyoshi for donating plasmids and Dr K. Yoshikawa (Doshisha University) for his helpful suggestion on the concept of mechanical deformation.

Competing interests

The authors declare no competing or financial interests.

Author contributions

K.F. designed and performed the majority of the experiments and co-wrote the manuscript with the assistance of A.K. H.T.-I. performed mathematical modeling. K.S. generated *Mark1* mutant mice. T.K. performed the experiments. A.K. designed experiments, interpreted results and co-wrote the manuscript.

Funding

This work was supported by Grants-in-Aid for Scientific Research (2013-2015; No. 25250018 to A.K.) and for Scientific Research on Innovative Areas (2011-2015; No. 23112004 to A.K.) from the Ministry of Education, Science and Culture of Japan and by grants from the Uehara Memorial Foundation.

Data availability

Microarray data have been deposited in NCBI Gene Expression Omnibus under accession number GSE83391 (https://www.ncbi.nlm.nih.gov/geo/query/acc.cgi?acc=GSE83391).

Supplementary information

Supplementary information available online at
http://dev.biologists.org/lookup/doi/10.1242/dev.141325.supplemental

References

Al Alam, D., Green, M., Tabatabai Irani, R., Parsa, S., Danopoulos, S., Sala, F. G., Branch, J., El Agha, E., Tiozzo, C., Voswinckel, R. et al. (2011). Contrasting expression of canonical Wnt signaling reporters TOPGAL, BATGAL and Axin2 (LacZ) during murine lung development and repair. *PLoS ONE* **6**, e23139.

Auth, T. and Gompper, G. (2009). Budding and vesiculation induced by conical membrane inclusions. *Phys. Rev. E* **80**, 031901.

Böhm, H., Brinkmann, V., Drab, M., Henske, A. and Kurzchalia, T. V. (1997). Mammalian homologues of C. elegans PAR-1 are asymmetrically localized in epithelial cells and may influence their polarity. *Curr. Biol.* **7**, 603-606.

Bryant, D. M., Roignot, J., Datta, A., Overeem, A. W., Kim, M., Yu, W., Peng, X., Eastburn, D. J., Ewald, A. J., Werb, Z. et al. (2014). A molecular switch for the orientation of epithelial cell polarization. *Dev. Cell* **31**, 171-187.

Chang, D. R., Martinez Alanis, D., Miller, R. K., Ji, H., Akiyama, H., McCrea, P. D. and Chen, J. (2013). Lung epithelial branching program antagonizes alveolar differentiation. *Proc. Natl. Acad. Sci. USA* **110**, 18042-18051.

Chao, C. M., El Agha, E., Tiozzo, C., Minoo, P. and Bellusci, S. (2015). A breath of fresh air on the mesenchyme: impact of impaired mesenchymal development on the pathogenesis of bronchopulmonary dysplasia. *Front Med.* **2**, 27.

Ciarletta, P., Balbi, V. and Kuhl, E. (2014). Pattern selection in growing tubular tissues. *Phys. Rev. Lett.* **113**, 248101.

Cohen, E. D., Ihida-Stansbury, K., Lu, M. M., Panettieri, R. A., Jones, P. L. and Morrisey, E. E. (2009). Wnt signaling regulates smooth muscle precursor development in the mouse lung via a tenascin C/PDGFR pathway. *J. Clin. Invest.* **119**, 2538-2549.

De Langhe, S. P., Sala, F. G., Del Moral, P.-M., Fairbanks, T. J., Yamada, K. M., Warburton, D., Burns, R. C. and Bellusci, S. (2005). Dickkopf-1 (DKK1) reveals that fibronectin is a major target of Wnt signaling in branching morphogenesis of the mouse embryonic lung. *Dev. Biol.* **277**, 316-331.

Desai, T. J., Brownfield, D. G. and Krasnow, M. A. (2014). Alveolar progenitor and stem cells in lung development, renewal and cancer. *Nature* **507**, 190-194.

Drasdo, D. (2000). Buckling instabilities of one-layered growing tissues. *Phys. Rev. Lett.* **84**, 4244-4247.

Fernandes, V. M., McCormack, K., Lewellyn, L. and Verheyen, E. M. (2014). Integrins regulate apical constriction via microtubule stabilization in the Drosophila eye disc epithelium. *Cell Rep.* **9**, 2043-2055.

Fumoto, K., Kikuchi, K., Gon, H. and Kikuchi, A. (2012). Wnt5a signaling controls cytokinesis by correctly positioning ESCRT-III at the midbody. *J. Cell Sci.* **125**, 4822-4832.

Goss, A. M., Tian, Y., Tsukiyama, T., Cohen, E. D., Zhou, D., Lu, M. M., Yamaguchi, T. P. and Morrisey, E. E. (2009). Wnt2/2b and β-catenin signaling are necessary and sufficient to specify lung progenitors in the foregut. *Dev. Cell* **17**, 290-298.

Harada, N., Tamai, Y., Ishikawa, T.-o., Sauer, B., Takaku, K., Oshima, M. and Taketo, M. M. (1999). Intestinal polyposis in mice with a dominant stable mutation of the beta-catenin gene. *EMBO J.* **18**, 5931-5942.

Hashimoto, S., Chen, H., Que, J., Brockway, B. L., Drake, J. A., Snyder, J. C., Randell, S. H. and Stripp, B. R. (2012). β-Catenin-SOX2 signaling regulates the fate of developing airway epithelium. *J. Cell Sci.* **125**, 932-942.

Hino, S., Tanji, C., Nakayama, K. I. and Kikuchi, A. (2005). Phosphorylation of beta-catenin by cyclic AMP-dependent protein kinase stabilizes beta-catenin through inhibition of its ubiquitination. *Mol. Cell Biol.* **25**, 9063-9072.

Kadzik, R. S., Cohen, E. D., Morley, M. P., Stewart, K. M., Lu, M. M. and Morrisey, E. E. (2014). Wnt ligand/Frizzled 2 receptor signaling regulates tube shape and branch-point formation in the lung through control of epithelial cell shape. *Proc. Natl. Acad. Sci. USA* **111**, 12444-12449.

Kikuchi, A., Yamamoto, H., Sato, A. and Matsumoto, S. (2011). New insights into the mechanism of Wnt signaling pathway activation. *Int. Rev. Cell Mol. Biol.* **291**, 21-71.

Kim, H. Y., Varner, V. D. and Nelson, C. M. (2013). Apical constriction initiates new bud formation during monopodial branching of the embryonic chicken lung. *Development* **140**, 3146-3155.

Lázaro-Diéguez, F., Cohen, D., Fernandez, D., Hodgson, L., van Ijzendoorn, S. C. D. and Müsch, A. (2013). Par1b links lumen polarity with LGN–NuMA positioning for distinct epithelial cell division phenotypes. *J. Cell Biol.* **203**, 251-264.

Lee, J.-Y. and Harland, R. M. (2007). Actomyosin contractility and microtubules drive apical constriction in Xenopus bottle cells. *Dev. Biol.* **311**, 40-52.

Luu, O., David, R., Ninomiya, H. and Winklbauer, R. (2011). Large-scale mechanical properties of Xenopus embryonic epithelium. *Proc. Natl. Acad. Sci. USA* **108**, 4000-4005.

Majumder, P., Aranjuez, G., Amick, J. and McDonald, J. A. (2012). Par-1 controls myosin-II activity through myosin phosphatase to regulate border cell migration. *Curr. Biol.* **22**, 363-372.

Martin, A. C. and Goldstein, B. (2014). Apical constriction: themes and variations on a cellular mechanism driving morphogenesis. *Development* **141**, 1987-1998.

Matsumoto, S., Kurimoto, T., Taketo, M. M., Fujii, S. and Kikuchi, A. (2016). The WNT/MYB pathway suppresses KIT expression to control the timing of salivary proacinar differentiation and duct formation. *Development* **143**, 2311-2324.

McDonald, J. A. (2014). Canonical and noncanonical roles of Par-1/MARK kinases in cell migration. *Int. Rev. Cell Mol. Biol.* **312**, 169-199.

Metzger, R. J., Klein, O. D., Martin, G. R. and Krasnow, M. A. (2008). The branching programme of mouse lung development. *Nature* **453**, 745-750.

Miller, M. F., Cohen, E. D., Baggs, J. E., Lu, M. M., Hogenesch, J. B. and Morrisey, E. E. (2012). Wnt ligands signal in a cooperative manner to promote foregut organogenesis. *Proc. Natl. Acad. Sci. USA* **109**, 15348-15353.

Morrisey, E. E. and Hogan, B. L. M. (2010). Preparing for the first breath: genetic and cellular mechanisms in lung development. *Dev. Cell* **18**, 8-23.

Mucenski, M. L., Wert, S. E., Nation, J. M., Loudy, D. E., Huelsken, J., Birchmeier, W., Morrisey, E. E. and Whitsett, J. A. (2003). beta-Catenin is required for specification of proximal/distal cell fate during lung morphogenesis. *J. Biol. Chem.* **278**, 40231-40238.

Nagai, T. and Honda, H. (2001). A dynamic cell model for the formation of epithelial tissues. *Philos. Mag. B* **81**, 699-719.

Nogawa, H. and Ito, T. (1995). Branching morphogenesis of embryonic mouse lung epithelium in mesenchyme-free culture. *Development* **121**, 1015-1022.

Rossi, A., Kontarakis, Z., Gerri, C., Nolte, H., Hölper, S., Krüger, M. and Stainier, D. Y. R. (2015). Genetic compensation induced by deleterious mutations but not gene knockdowns. *Nature* **524**, 230-233.

Savin, T., Kurpios, N. A., Shyer, A. E., Florescu, P., Liang, H., Mahadevan, L. and Tabin, C. J. (2011). On the growth and form of the gut. *Nature* **476**, 57-62.

Shu, W., Jiang, Y. Q., Lu, M. M. and Morrisey, E. E. (2002). Wnt7b regulates mesenchymal proliferation and vascular development in the lung. *Development* **129**, 4831-4842.

Shu, W., Guttentag, S., Wang, Z., Andl, T., Ballard, P., Lu, M. M., Piccolo, S., Birchmeier, W., Whitsett, J. A., Millar, S. E. et al. (2005). Wnt/β-catenin signaling acts upstream of N-myc, BMP4, and FGF signaling to regulate proximal–distal patterning in the lung. *Dev. Biol.* **283**, 226-239.

Sunagawa, G. A., Sumiyama, K., Ukai-Tadenuma, M., Perrin, D., Fujishima, H., Ukai, H., Nishimura, O., Shi, S., Ohno, R., Narumi, R. et al. (2016). Mammalian reverse genetics without crossing reveals Nr3a as a short-sleeper gene. *Cell Rep.* **14**, 662-677.

Takigawa-Imamura, H., Morita, R., Iwaki, T., Tsuji, T. and Yoshikawa, K. (2015). Tooth germ invagination from cell–cell interaction: Working hypothesis on mechanical instability. *J. Theor. Biol.* **382**, 284-291.

Treutlein, B., Brownfield, D. G., Wu, A. R., Neff, N. F., Mantalas, G. L., Espinoza, F. H., Desai, T. J., Krasnow, M. A. and Quake, S. R. (2014). Reconstructing lineage hierarchies of the distal lung epithelium using single-cell RNA-seq. *Nature* **509**, 371-375.

Varner, V. D., Gleghorn, J. P., Miller, E., Radisky, D. C. and Nelson, C. M. (2015). Mechanically patterning the embryonic airway epithelium. *Proc. Natl. Acad. Sci. USA* **112**, 9230-9235.

Wang, Z., Shu, W., Lu, M. M. and Morrisey, E. E. (2005). Wnt7b activates canonical signaling in epithelial and vascular smooth muscle cells through interactions with Fzd1, Fzd10, and LRP5. *Mol. Cell. Biol.* **25**, 5022-5030.

Weaver, M., Dunn, N. R. and Hogan, B. L. (2000). Bmp4 and Fgf10 play opposing roles during lung bud morphogenesis. *Development* **127**, 2695-2704.

Yang, J., Hernandez, B. J., Martinez Alanis, D., Narvaez Del Pilar, O., Vila-Ellis, L., Akiyama, H., Evans, S. E., Ostrin, E. J. and Chen, J. (2016). The development and plasticity of alveolar type 1 cells. *Development* **143**, 54-65.

Yonemura, S., Wada, Y., Watanabe, T., Nagafuchi, A. and Shibata, M. (2010). α-Catenin as a tension transducer that induces adherens junction development. *Nat. Cell Biol.* **12**, 533-542.